Materials Letters 106 (2013) 304–307

Contents lists available at SciVerse ScienceDirect

Materials Letters

journal homepage: www.elsevier.com/locate/matlet

# Tungsten doping magnetic iron oxide and their enhanced lithium Ćion storage properties

Jinxue Guo, Lei Chen, Xiao Zhang*, Xiaoyu Zhou, Guangjin Wang, Bin Jiang

*College of Chemistry and Molecular Engineering, Qingdao University of Science and Technology, Qingdao 266042, China*

ARTICLE INFO

*Article history:*
Received 15 March 2013
Accepted 13 May 2013
Available online 22 May 2013

*Keywords:*
Energy storage and conversion
Magnetic materials
W-doped $Fe_3O_4$
XPS

ABSTRACT

This work presents a hydrothermal synthesis of W-doped $Fe_3O_4$ nanoparticles. The results indicate that $Fe^{2+}$ but not $Fe^{3+}$ is substituted with $W^{6+}$. Both undoped and doped $Fe_3O_4$ show ferromagnetic behaviors. The magnetism of $Fe_3O_4$ decreases from 7.2 emu $g^{-1}$ to 5.0 emu $g^{-1}$ after doping, because the super-exchange interactions between $Fe^{2+}$ and $Fe^{3+}$ are hindered by W. Interestingly, W-doped $Fe_3O_4$ exhibits improved reversible capacity of 629 mAh $g^{-1}$ in comparison with 341.3 mAh $g^{-1}$ of pure $Fe_3O_4$ for their first charge/discharge cycle, and shows higher initial Coulombic efficiency of 86.1%. Moreover, better cyclic stability has been obtained for W-doped $Fe_3O_4$. The W-doped $Fe_3O_4$ would be a candidate in applications of lithium ion batteries, magnetic materials, and other areas.



## 1. Introduction

$Fe_3O_4$ has been extensively studied for its unique properties and various applications of magnetic separation [1], magnetic response imaging [2], targeted drug delivery [3], and water treatment [4]. It has also been considered as a promising anode for lithium ion batteries (LIBs) due to its high theoretical capacity (~920 mAh $g^{-1}$), natural abundance, low cost, and environmental benignity [5].

Recently, it has been demonstrated that the substitution of Fe with another metal element will reform the crystal structure of $Fe_3O_4$ and tune their magnetic and electrical properties, extending their application range. Various divalent metallic elements such as Mn [6], Zn [7], Co [8] and Ni [9] have been employed for the substitution. For example, Hwang et al. have synthesized Mn-doped $Fe_3O_4$ nanowire arrays and revealed that Mn substitution reduced magnetization of $Fe_3O_4$ [6]. Though the magnetic properties hindered by the metal doping have been studied widely, the effect of metal doping on the lithium ion storage property of $Fe_3O_4$ nanostructures, to our knowledge, has not been revealed. Thus, a study of the effect of metal doping on the properties of $Fe_3O_4$, especially on the lithium ion storage property, is desirable for both fundamental scientific interest and its potential application.

Tungsten oxide was chosen for the substitution of $Fe_3O_4$, because it is known as a good anode material for LIBs [10]. A simple hydrothermal method was developed to synthesize W-doped $Fe_3O_4$ nanoparticles at a large scale. The detailed investigations of W-doped $Fe_3O_4$ and pure $Fe_3O_4$ nanoparticles have been performed. In this study, we are devoted to demonstrating how the doping of W influences the magnetic and electrochemical properties of $Fe_3O_4$ nanoparticles.

## 2. Experimental

*Synthesis of W-doped $Fe_3O_4$:* $Na_2WO_4$ solution (0.01 M) was added into a mixing solution of $FeSO_4$ (0.01 M) and SDBS (0.02 M). The pH value was tuned to 10 with NaOH. Resultant solution was transferred into autoclaves, and heated at 180 °C for 12 h. The precipitates were obtained with centrifuge. Pure $Fe_3O_4$ nanoparticles were synthesized following the same route without the addition of $Na_2WO_4$ for comparison.

*Characterization:* The samples were characterized with powder X-ray diffraction (XRD) by a Philips X′-pert X-ray diffractometer, transmission electron micrographs (TEM) on a FEI TECNAI F30, and the energy dispersive spectroscopy (EDS) probe equipped on a JEOL JSM-6700 F scanning electron microscope (SEM). The magnetic properties were measured with a high sensitivity vibrating sample magnetometer (Model 7404, Lakeshore) at room temperature. X-ray photoelectron spectroscopy (XPS) was carried out on a RBD upgraded PHI-5000c ESCA system (Perkin Elmer) with Mg Kα radiation ($h\nu = 1253.6$ eV).

*Electrochemical measurements:* The electrochemical tests were carried out with a CR2016-type coin cell. Metallic lithium was used as negative electrodes. The working electrode was fabricated by compressing a mixture of active materials, acetylene black and polyvinylidene fluoride in a weight ratio of 75:15:10 onto a copper foil, and dried at 120 °C for 24 h under vacuum. The Clegard 2300

* Corresponding author. Tel.: +86 532 84022681; fax: +86 532 84023927.
*E-mail address:* zhx1213@126.com (X. Zhang).

0167-577X/$ - see front matter © 2013 Elsevier B.V. All rights reserved.
http://dx.doi.org/10.1016/j.matlet.2013.05.046

microporous film was used as separator. The electrolyte solution was 1 M $LiPF_6$ dissolved in a mixture of ethylene carbonate/dimethyl carbonate/ethyl methyl carbonate (1:1:1). The cell assembly was operated in a glove box filled with pure argon. Charge–discharge experiments were performed between 0.01 and 3 V on a LAND CT2001A Battery Cycler.

## 3. Results and discussion

Fig. 1a shows that all diffraction peaks of pure $Fe_3O_4$ can be indexed to a pure, well-crystalline, face-centered cubic spinel structure (JCPDS card no. 65-3107). The XRD pattern of W-doped $Fe_3O_4$ is approximately similar to those of pure $Fe_3O_4$. But all peaks of W-doped $Fe_3O_4$ shift slightly toward lower angles, suggesting an increase of lattice constants. It is due to the substitutions of Fe ions with bigger W ions in the host lattice, which agrees well with the previous reports [6]. The enlargement of the diffraction intensity of the strongest peak of (311) plane is presented in Fig. 1b to display this shift more clearly. It is shown that the position of (311) peak of W-doped $Fe_3O_4$ shifts by 0.12° (2$\theta$), providing a strong evidence of successfully W doping in $Fe_3O_4$ host matrix. The atomic ration of Fe to W element was determined to be 3:1 according to the EDS analysis.

XPS measurements were performed to further investigate their crystal phase. In Fig. 1c, there are two characteristic peaks located at 710.6 and 724 eV observed for pure $Fe_3O_4$, which should be assigned to Fe $2p_{3/2}$ and Fe $2p_{1/2}$, respectively [11]. In comparison, the Fe $2p_{3/2}$ and Fe $2p_{1/2}$ peaks of W-doped $Fe_3O_4$ shift to higher energy region by 2.4 and 2.2 eV respectively, further confirming the successful doping of W. It is believed that Fe 2p peaks located at higher binding energy display higher oxidation state. The higher binding energies of Fe 2p peaks for W-doped $Fe_3O_4$ indicate that Fe in W-doped $Fe_3O_4$ possesses higher oxidation state. So it can be concluded that there is less amount of $Fe^{2+}$ and higher $Fe^{3+}/Fe^{2+}$ ratio in W-doped $Fe_3O_4$, attributing to the substitution of $Fe^{2+}$ with W cations. Fig. 1d shows the XPS spectra of W 4f in W-doped $Fe_3O_4$. The W 4f peak is separated into two peaks by the same peak fitting deconvolution technique. The peaks at 35.8 and 37.6 eV can be assigned to W 4 $f_{7/2}$ and W 4 $f_{5/2}$ respectively and $\Delta E$ is 1.8 eV. According to standard binding energies and reported values [12], the exacting form of W ions in the W-doped $Fe_3O_4$ is $W^{6+}$.

Fig. 2a and c shows that both the products are particles with similar diameters ranging from 20–200 nm, indicating that the W doping has no significant influence on their morphology and size. As is shown in the high-resolution TEM images (Fig. 2 b and d), all the products are well crystallized and exhibit clear crystal lattices. Pure $Fe_3O_4$ (Fig. 2 b) shows interplanar spacing of 0.486 nm, which is consistent with the spacing (0.484 nm) of (111) planes for face-centered cubic spinel $Fe_3O_4$. W-doped $Fe_3O_4$ shows higher interplanar spacing of 0.497 nm (Fig. 2 d), attributing to substitution of Fe with bigger W.

The hysteresis loops (Fig. 3) show that the specific saturation magnetization ($M_s$) of W-doped $Fe_3O_4$ is about 5.0 emu $g^{-1}$, which is lower than that of pure $Fe_3O_4$ (7.2 emu $g^{-1}$). As we all know, the magnetism of $Fe_3O_4$ arises from the superexhcange interactions among the $Fe^{3+}$ and $Fe^{2+}$. The substitution of $Fe^{2+}$ with $W^{6+}$ will hinder the superexchange and results in the decrease of $M_s$. The enlarged hysteresis loops are shown in the inset of Fig. 3, which shows that the coercive forces ($H_c$) are 200 Oe for W-doped $Fe_3O_4$ and 150 Oe for pure $Fe_3O_4$. The remanent magnetizations ($M_r$) are 0.64 emu $g^{-1}$ for W-doped $Fe_3O_4$ and 1.09 emu $g^{-1}$ for pure $Fe_3O_4$, revealing their weak ferromagnetic behaviors.

Fig. 4a presents the potential profiles in the 1st cycle of pure $Fe_3O_4$ and W-doped $Fe_3O_4$. The obvious extended potential plateau from ~0.8 V to 0.01 V is observed for both two electrode materials,

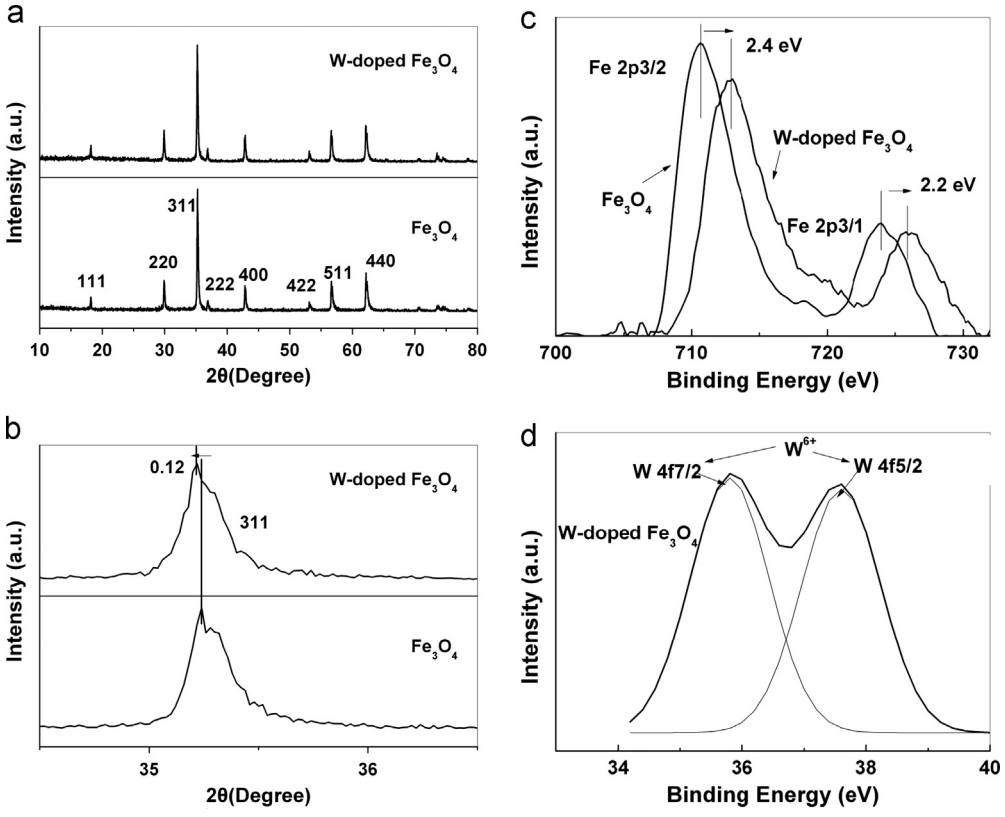


**Fig. 1.** (a) XRD patterns of pure $Fe_3O_4$ and W-doped $Fe_3O_4$ nanoparticles. (b) Magnified XRD (311) peaks. (c) XPS spectra of Fe 2p of the products. (d) W 4f peak of W-doped $Fe_3O_4$ nanoparticles.